Automated Cell Counting in Bürker Chamber

Karel Štěpka

Centre for Biomedical Image Analysis, Faculty of Informatics,
Masaryk University, Brno, Czech Republic

Abstract. Estimating the number of blood cells in a sample is an important task in biological research. However, manual counting of cells in microscopy images of counting chambers is very time-consuming. We present an image processing method for detecting the chamber grid and the cells, based on their similarity to an automatically selected sample cell. Due to this approach, the method does not depend on specific cell structure, and can be used for blood cells of different species without adjustments. If deemed appropriate, user interaction is allowed to select the sample cell and adjust the parameters manually. We also present the accuracy and speed evaluation of the method.

Keywords: cell counting, image analysis, hemocytometer.

1 Introduction

The number of erythrocytes per unit of volume of blood is an important factor in many biological studies. It is linked to the specimen's age, health condition, diet, hormone levels, or states such as hypoxia [1–3].

A routine and well-established method for estimating this value is using a counting chamber (hemocytometer). The counting chamber is filled with a diluted blood sample and placed under an optical microscope. Knowing the dimensions of the chamber and of the grid of fine, precisely spaced lines etched in the bottom of the chamber, we can estimate the number of blood cells per unit of volume by counting the cells in different segments of the grid. However, manual counting is very time-consuming, and automation is therefore desirable.

Automated counting of erythrocytes in a general case is however made difficult by the large variability in the appearance of erythrocytes in various species. Differences include the size, shape, and even the internal structure of the cells (mammal erythrocytes are non-nucleated). This is illustrated in Fig. 1. Furthermore, in some studies, the images can be acquired in field conditions, resulting in a relatively low quality that can vary over the image set. Because of this, the detection cannot rely for example on the relative intensity or contrast of the cells, the background, and the chamber grid.

In this work, we present a new method for automated counting of cells in bright field microscopy images of blood samples in Bürker chamber. An example image is shown in Fig. 2; the images were taken under varying light conditions, were JPEG-compressed, and we can note the uneven illumination. One of the

J.-K. Kämäräinen and M. Koskela (Eds.): SCIA 2013, LNCS 7944, pp. 236–245, 2013.

challenges was to make the method universally applicable to this type of images, without tailoring it to a specific chamber or cell appearance.

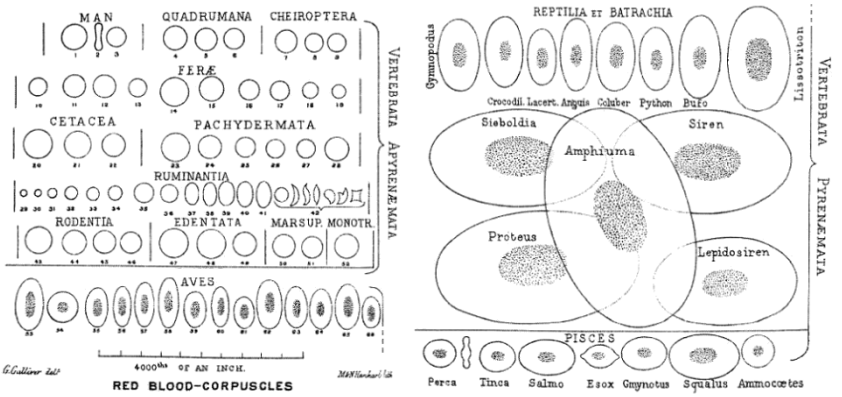

Fig. 1. Red blood cells of various species. Left, top to bottom: mammals (non-nucleated cells), birds. Right, top to bottom: reptiles and amphibians, fish. (Adapted from [4].)

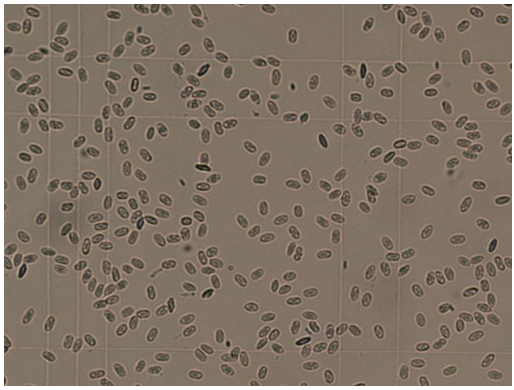

Fig. 2. Avian erythrocytes in Bürker counting chamber (top left quarter of the whole image). In this image, the grid lines appear brighter than the background.

2 Previous Research

Various methods have been used for computerized cell counting. A common approach is intensity thresholding, used for example by Vinkler et al. in a semi-automatic method in [5]. Generally, intensity thresholding can yield good results if the cell, background, and grid intensities are well-separated.

A different class of methods utilizes edge detection and is less dependent on the intensity relations, such as [6], based on a modified Laplacian filter, or [7], which starts by using the Prewitt operator. Another possibility is a model-based approach; for example, Debeir et al. [8] used a model-based method for cell detection and tracking in phase contrast images.

A common problem in cell detection is splitting of clusters of touching cells. In [6, 9], such clusters were split using a distance map approach. Camisard et al. [10] utilized edge map and pattern matching with user-selected templates. In some works, clusters were only identified, without splitting [7]. Work [7] also detects the chamber grid, but relies on its contrast being relatively high (similar to that of the cells), and also on a precise angular alignment.

Several commercial, closed-source hardware solutions exist. In these solutions, the image acquisition is handled by the device, resulting in non-varying image quality, which allows the use of specifically tuned algorithms.

To our knowledge, no universal method is however available for simultaneous detection of the chamber grid and counting of cells of different species in bright field images of counting chambers taken under varying lighting or focusing conditions, and many laboratories routinely use manual counting.

3 Algorithm

Our approach to the task of counting the cells consists of pre-processing followed by three relatively well-separated steps: (1) grid detection, (2) finding a sample cell, and (3) cell detection using similarity to the sample cell.

During pre-processing, we convert the image to greyscale. The noise is suppressed by Gaussian blurring, and the contrast and intensity are enhanced by applying the transformation described in [11].

Uneven illumination and large smudges are removed by subtracting a blurred copy of the image from the image itself, yielding an image with background intensity near zero. Depending on the lighting conditions during acquisition, the grid intensity can be lower, equal, or higher than that of the cells. We can therefore simplify and unify the following steps by taking the absolute value of this image, normalized to $\langle 0; 1 \rangle$. Values near 0 correspond to the chamber background, higher values to the cells and the grid.

3.1 Chamber Grid Detection

A common method for detection of linear image structures is the Hough transform (HT). To use it, we need to address several concerns. An ideal input for HT consists mostly of the lines, with only a few other non-zero pixels. However, due to the variability of images and light conditions, we cannot always distinguish between the grid lines and cells based on their intensity. Furthermore, the grid may be partially obstructed, and its contrast may be very low compared to that of the cells. Lastly, depending on the lighting and the chamber itself, a single grid line can appear "doubled", i.e. as two parallel lines instead of one.

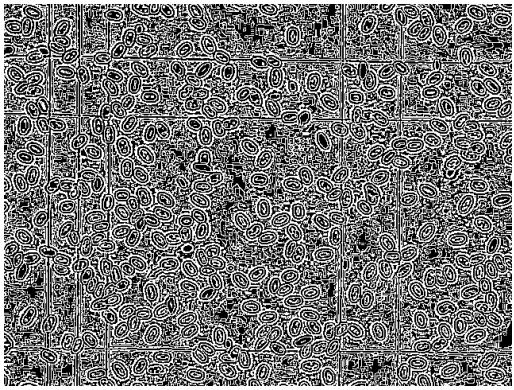

Fig. 3. Thresholded second derivative of the pre-processed image

We addressed the problem of low contrast by taking the second derivative of the image, and thresholding the result with a relatively low threshold, thus extracting the edges. As we can see in Fig. 3, this does not distinguish between the cells and the grid, but it allows us to separate these structures from the background, regardless of their relative contrast.

Following this, the horizontal and vertical grid lines are processed separately. The roughly-horizontal (or roughly-vertical) structures are extracted by morphological erosion with a linear structuring element (SE). The length of the SE is linked to the angular tolerance – with shorter element, the tolerance is higher, but it becomes more difficult to remove all cells. We found that with the length corresponding to 1 % of the image height, the method successfully detects lines deviating by as much as 5° from the true horizontal or vertical. In the available data, the actual deviation never exceeded 2°.

The erosion removes most of the non-zero pixels corresponding to the cells, leaving the grid lines, as shown in Fig. 4. We can clearly see the multiplied lines, resulting from the second derivative peaks on both sides of the actual lines, and also from the lines themselves being "doubled" in this particular image.

The eroded images are then used as the input for the progressive probabilistic Hough transform (PPHT), described in [12]. Using PPHT is less time-consuming than the full Hough transform, while still providing good results. For the accumulator, the resolution of $\Delta\theta = 0.5°$ and $\Delta\rho = 1$ pixel was used.

Outliers with respect to the line angle are discarded (this applied to less than 0.5 % of the detected lines in the test data), and the lines close to each other are merged by averaging their parameters. Since both the second derivative peaks, and the multiple lines appearing due to the "doubling" are placed symmetrically around the actual line positions, this preserves the line locations, while removing the duplicates.

After the merging, the lines are labeled according to their position in the Bürker chamber, based on their relative spacing. Assuming a sufficiently large part of the chamber is imaged (at least one large and one small segment of

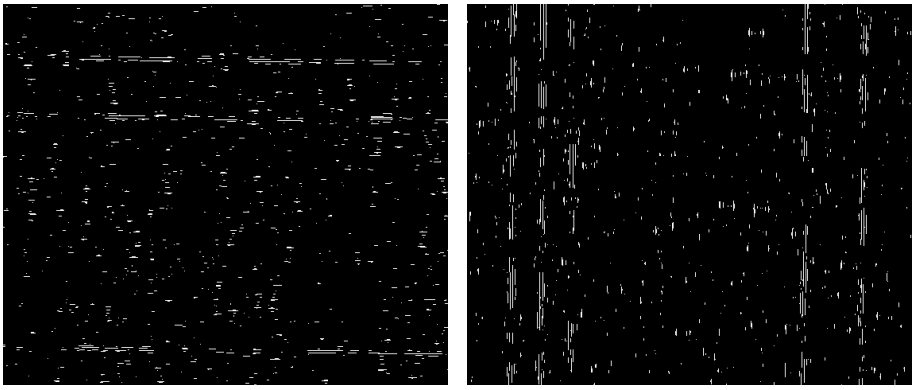

Fig. 4. Result of erosion with a horizontal (left) and a vertical (right) linear SE

the grid in both dimensions), this can be done by examining the following five distance ratios: $1:4$, $1:5$, $1:1:8$, $1:1:10$, $1:1$

Due to the regular structure of the Bürker chamber, the procedure is successful even if some of the lines are missing in the HT result. In such case, their supposed positions can be calculated, and the missing lines added.

3.2 Sample Cell Identification

Due to the variablility in the appearance of red blood cells of different species, it is difficult to search for them using some universal description. Instead, we seek to identify a sample cell in the image, and then detect other cells based on their visual similarity to the sample. As the sample, we want to select a square image subwindow meeting the following criteria:

1. The subwindow contains only one cell.
2. The cell is well isolated from the surrounding objects.
3. The cell is of average size.
4. The subwindow fits closely to the cell.
5. The cell does not touch the image border.

To extract the sample, we first create a binary mask of all candidates by adaptive thresholding of the Gaussian-blurred pre-processed image. Gaussian blurring serves to suppress the influence of small variations in the internal structure of individual cells. The thresholding parameters are set liberally, so that the mask created from the blurred cells covers all of them without cropping. The adaptivity of the thresholding allows to compensate for different contrast in different areas of the image.

The cell mask is then processed by morphological opening with a small disk-shaped SE, in order to separate some of the cells and remove small protrusions and components corresponding to debris or other artifacts, as seen in Fig. 5.

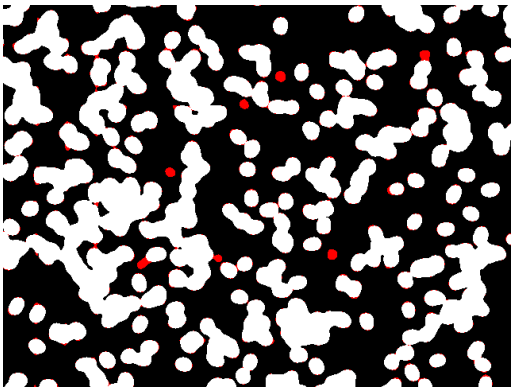

Fig. 5. Cell mask. Red parts have been removed by morphological opening.

Connected components touching the border are then discarded (addressing criterion (5)), together with the non-convex components. This utilizes the observation that clusters of touching cells are only rarely convex, partially addressing criteria (1) and (2). After discarding these components, only individual cells and small convex clusters remain. By further considering only those components whose area is within a specified range of the median area, we make sure no outliers (corresponding to small debris or convex clusters), are selected. This addresses (1) and (3), and is illustrated in Fig. 6. Finally, we select the sample as one of those remaining components whose bounding box is not intersected by other components of the mask (addressing (2) and (4)).

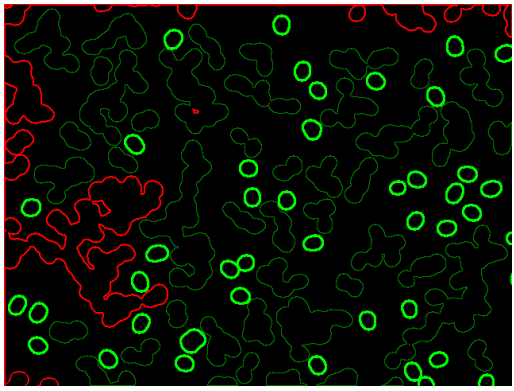

Fig. 6. Thin red contours show the components at the image border (only top left quarter of the image is shown), or component holes. Thin green contours show components discarded due to non-convexity. Thick green lines show the remaining candidates. Note the large candidate in the lower part of the figure, left from the center. This is a convex cluster of two cells, and will be removed by applying the "median area" criterion.

3.3 Cell Matching

To detect the individual cells, we calculated the correlation coefficient response for different possible rotations of the sample in each image pixel. The correlation coefficient of images f and g in point (s,t) is defined as

$$CCOEFF_{f,\,g}(s,t) = \sum_{u,v} \big(f(s+u,t+v) - \overline{f}\big)\big(g(u,v) - \overline{g}\big)\,, \tag{1}$$

where $\overline{f}$ and $\overline{g}$ denote the mean intensity of f and g, respectively.

In total, 16 rotation steps covering 180° were used (example shown in Fig. 7). The computation speed was optimized by performing the calculations in Fourier domain, with the extent of necessary Fourier transform-related calculations being $16 \times FFT_{sample} + 1 \times FFT_{image} + 16 \times IFFT_{image}$
(where FFT and IFFT denote fast Fourier transform and its inverse, and the lower index indicates either the sample cell region, or the whole image).

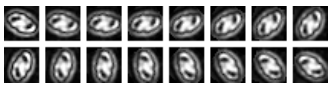

Fig. 7. Rotation steps of the sample cell region, covering 180°

Pixel-wise maximum of the responses for each rotation step was then combined with an eroded version of the cell mask from the previous phase. This yielded an image whose local maxima lay inside the cells, in places with maximum similarity to the sample.

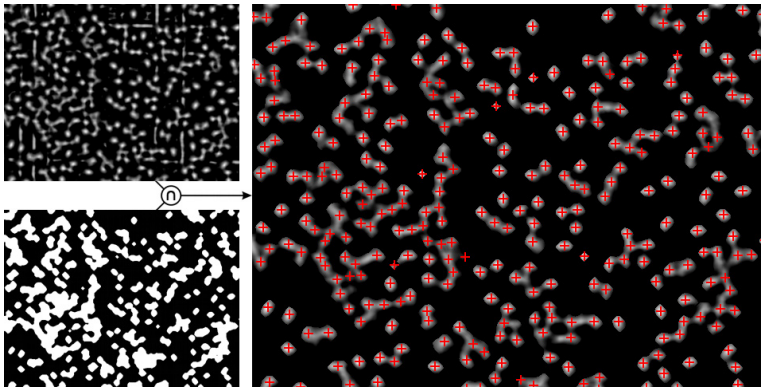

Fig. 8. Sample matching result. Local maxima of the correlation coefficient higher than the specified threshold are superimposed as red cross marks.

Finally, we calculated the extended maxima (EMAX) transform as the regional maxima of the HMAX transform, as described in [13]. This extracted the local maxima with sufficient contrast. Finding these maxima allowed us to detect the cells even when they were a part of a cluster of touching cells. Unlike distance maps, this allows us to detect the cells even if they form a convex or almost-convex cluster. By labeling the results and merging the marks whose distance from each other was smaller than one half of the expected cell size (which was determined during the sample extraction step in 3.2), we obtained the final cell markers for counting, as shown in Fig. 8.

4 Performance Evaluation

Using blood sample images of common rosefinch, house mouse, great tit, and chicken, taken by a bright field optical microscope during field research, we evaluated the performance of the method. The input JPEG images had the size of 1280×960 pixels, covering roughly 0.55 mm^2 area of the chamber.

The results are shown in Fig. 9. The black bars show the *ground truth* numbers of cells manually counted by an expert, while the blue and green bars show the fully automatic and semi-automatic counting, respectively. In fully automatic cases, only the default parameter values were used for all images; in semi-automatic cases, the user was allowed to adjust the method's parameters and select the sample cell manually, if deemed appropriate.

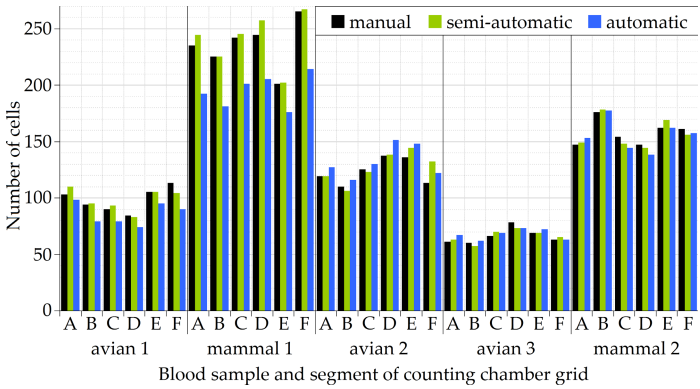

Fig. 9. Comparison of manual (black), semi-automatic (green), and fully automatic (blue) counting results for different blood samples

We see that the fully automatic counting underestimated the number of cells in highly-concentrated blood samples, and that this case required the user interaction to yield more accurate results. In lower-concentration samples, the fully automatic results followed the ground truth much more closely.

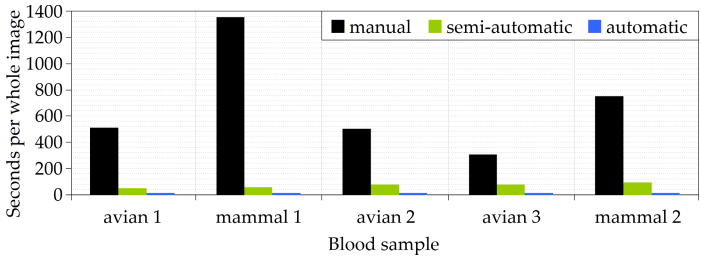

Fig. 10. Comparison of manual (black), semi-automatic (green), and fully automatic (blue) counting speed on a single-core, 2.6 GHz processor

The speed of the detection is shown in Fig. 10. In the semi-automatic cases, in which the detection was usually run multiple times with different parameters, this represents the sum of all detections and the time during which the user was adjusting the parameters. We see that the fully automatic detection is the fastest, requiring approximately 13 seconds per image on a single-core, 2.6 GHz processor. The semi-automatic detection, despite utilizing user input, is still significantly faster than the manual counting.

We can note that in practical applications, higher dilution of the sample (combined with taking images of more grid segments to maintain the statistical significance) would alleviate the underestimation problem mentioned above, while still offering a considerable speedup when compared to manual counting applied to high-concentration samples.

5 Conclusion

We presented a new universal method for counting of erythrocytes in bright field images of Bürker chamber. The method, consisting of several relatively separate steps, first automatically detects the chamber grid, regardless of its relative intensity and contrast when compared to the cells. Due to the use of morphological erosion, the robustness of this step is ensured even when the grid is partially obstructed by cells.

A sample cell is then identified, and other cells are detected based on the similarity to the sample, making the method applicable to blood samples of different species without any specific adjustments. Detecting peaks of the similarity function also helps to detect touching cells.

User interaction can be allowed to select the sample cell, or adjust the method parameters. The number of adjustable parameters has been limited to two: the required correlation coefficient response (intuitively understandable as a "strictness" of the method), and the pre-processing blur amount.

Testing on mammal (non-nucleated) and avian (nucleated) cells showed that even in the fully automatic setting, the method yields acceptable results for low to medium cell concentrations, while being significantly faster than the manual

approach. In the case of semi-automatic counting, which allows user interaction, the speedup is still significant, and the results match the ground truth closely even in high-concentration cases. A demonstration application can be downloaded from http://is.muni.cz/www/172454/cc.zip

Acknowledgments. We wish to thank Marek Vinkler and the Biodiversity Research Group, Faculty of Science, Charles University, for providing the images.

References

1. Campbell, T.W., Ellis, C.K.: Avian and Exotic Animal Hematology and Cytology, 3rd edn. Blackwell Publishing, Ames (2007)
2. Jensen, F.: Regulatory Volume Decrease in Carp Red Blood Cells: Mechanisms and Oxygenation-Dependency of Volume-Activated Potassium and Amino Acid Transport. Journal of Experimental Biolog. 198(1), 155–165 (1995)
3. Ishikawa-Sekigami, T., Kaneko, Y., Okazawa, H., Tomizawa, T., Okajo, J., Saito, Y., Okuzawa, C., Sugawara-Yokoo, M., Nishiyama, U., Ohnishi, H., Matozaki, T., Nojima, Y.: SHPS-1 Promotes the Survival of Circulating Erythrocytes Through Inhibition of Phagocytosis by Splenic Macrophages. Blood 107(1), 341–348 (2006)
4. Gulliver, G.: On the size and shape of red corpuscles of the blood of vertebrates, with drawings of them to a uniform scale, and extended and revised tables of measurements. Proceedings of the Royal Society of London, 474–495 (1875)
5. Vinkler, M., Schnitzer, J., Munclinger, P., Votýpka, J., Albrecht, T.: Haematological health assessment in a passerine with extremely high proportion of basophils in peripheral blood. Journal of Ornithology 151, 841–849 (2010)
6. Loukas, C.G., Wilson, G.D., Vojnovic, B., Linney, A.: An image analysis-based approach for automated counting of cancer cell nuclei in tissue sections. Cytometry 55A(1), 30–42 (2003)
7. Prasad, B., Badawy, W.: High throughput algorithm for leukemia cell population statistics on a hemocytometer. In: IEEE Biomedical Circuits and Systems, pp. 142–145 (2007)
8. Debeir, O., Camby, I., Kiss, R., Van Ham, P., Decaestecker, C.: A model-based approach for automated in vitro cell tracking and chemotaxis analyses. Cytometry 60A(1), 29–40 (2004)
9. Nilsson, B., Heyden, A.: Segmentation of complex cell clusters in microscopic images: Application to bone marrow samples. Cytometry 66A(1), 24–31 (2005)
10. Camisard, V., Brienne, J.-P., Baussart, H., Hammann, J., Suhr, H.: Inline characterization of cell concentration and cell volume in agitated bioreactors using in situ microscopy: Application to volume variation induced by osmotic stress. Biotechnology and Bioengineering 78(1), 73–80 (2002)
11. Streidt, W.D.: Brightness/Contrast Code (1999), `http://visca.com/ffactory/archives/5-99/msg00021.html` (January 16, 2013)
12. Matas, J., Galambos, C., Kittler, J.: Progressive Probabilistic Hough Transform for Line Detection. In: IEEE Computer Vision and Pattern Recognition, pp. 1554–1560 (June 1999)
13. Vincent, L.: Morphological Grayscale Reconstruction in Image Analysis: Applications and Efficient Algorithms. IEEE Transactions on Image Processing 2, 176–201 (1993)